Scientific Paper / Artículo Científico

UNIVERSIDAD POLITÉCNICA SALESIANA ECUADOR
INGENIUS
Revista de Ciencia y Tecnología
https://doi.org/10.17163/ings.n36.2026.07
pISSN: 1390-650X / eISSN: 1390-860X

Influence of cabin temperature and compressor speed on the performance of an automotive air conditioning system

Influencia de la temperatura del habitáculo y la velocidad del compresor en el rendimiento del sistema de aire acondicionado automotriz

Iván M. Ashqui-Cuvi[1], Klever S. Morales-Morales[1], Daniela C. Vásconez-Núñez[2], Fernando M. Tello-Oquendo[3,*], Fabián C. Gunsha-Maji[3]

Received: 16-11-2025, Received after review: 09-03-2026, Accepted: 21-04-2026, Published: 01-07-2026

Abstract

This study examines the influence of compressor speed and cabin temperature on the performance of an automotive air conditioning system. An experimental test bench was developed with a compressor coupled to a variable-speed electric motor and equipped with pressure, temperature, and air velocity sensors, as well as a thermal chamber to regulate the temperature of the air entering the evaporator. A thermodynamic model was also implemented to calculate the compressor operating parameters and evaluate system performance. The results show that increasing the compressor speed from 900 to 2800 rpm raises the refrigerant mass flow rate and cooling capacity by up to 50.3 % and 22.4 %, respectively, thereby improving the cooling capacity. However, this increase also raises power consumption from 0.287 to 0.878 kW and nearly doubles fuel consumption, reaching 0.54 L/h at a cabin temperature of 45 °C. In addition, isentropic efficiency, volumetric efficiency, and the coefficient of performance decrease by up to 22.66%, 44%, and 61.27%, respectively, while the compressor discharge temperature exceeds 80 °C at high operating speeds. Finally, correlations are proposed to estimate compressor efficiencies, and fuel consumption is calculated considering the powertrain efficiencies of a gasoline-powered internal combustion engine vehicle.

Keywords: compressor speed, cabin temperature, volumetric efficiency, isentropic efficiency, coefficient of performance, air conditioning

Resumen

Este artículo analiza la influencia de la velocidad del compresor y la temperatura del habitáculo en el rendimiento del sistema de aire acondicionado automotriz. Para ello, se construyó un banco experimental con un compresor acoplado a un motor eléctrico de velocidad variable, equipado con sensores de presión, temperatura y velocidad del aire, así como una caja térmica para regular la temperatura del aire de entrada al evaporador. Además, se implementó un modelo termodinámico para calcular los parámetros de funcionamiento del compresor y el desempeño del sistema. Los resultados muestran que, al incrementar la velocidad del compresor de 900 a 2800 rpm, el flujo másico de refrigerante y la capacidad frigorífica aumentan hasta en un 50.3 % y un 22.4 %, respectivamente, lo que mejora la capacidad de enfriamiento. Sin embargo, también se incrementan la potencia consumida de 0.287 a 0.878 kW, y el consumo de combustible, que llega a duplicarse hasta 0.54 L/h a 45 °C de temperatura en el habitáculo. Asimismo, se observa una disminución de la eficiencia isentrópica del 22.66 %, de la eficiencia volumétrica del 44 % y del coeficiente de desempeño (COP) de hasta 61.27 %, junto con un incremento de la temperatura de descarga del compresor por encima de 80 °C a altas velocidades. Finalmente, se proponen correlaciones para el cálculo de las eficiencias del compresor y se estima el consumo de combustible considerando las eficiencias del tren motriz de un vehículo con motor de combustión interna a gasolina.

Palabras clave: velocidad del compresor, temperatura del habitáculo, eficiencia volumétrica, eficiencia isentrópica, coeficiente de desempeño, aire acondicionado.

[1]Investigador independiente, Ecuador.
[2]Grupo de investigación INVELECTRO, Carrera de Ingeniería Industrial, Facultad de Mecánica, Escuela Superior Politécnica de Chimborazo (ESPOCH), Riobamba, Ecuador.
[3,*]Grupo de investigación INVELECTRO, Carrera de Ingeniería Automotriz, Facultad de Mecánica, Escuela Superior Politécnica de Chimborazo (ESPOCH), Riobamba, Ecuador. Corresponding author ✉: fernando.tello@espoch.edu.ec.

Suggested citation: I. M. Ashqui-Cuvi, K. S. Morales-Morales, D.C. Vásconez-Núñez, F. M. Tello-Oquendo and F. C. Gunsha-Maji "Influence of cabin temperature and compressor speed on the performance of an automotive air conditioning system," *Ingenius, Revista de Ciencia y Tecnología*, N.° 36, pp. 84-97, 2026, DOI: https://doi.org/10.17163/ings.n36.2026.07.

1. Introduction

The automotive air conditioning (A/C) system removes heat from the air inside the vehicle to maintain thermal comfort, particularly under hot climate conditions. Thermal comfort refers to the state of physical and psychological satisfaction experienced under environmental conditions typically associated with temperatures between 20 and 40 °C and relative humidity levels ranging from 30% to 60% [1]. The A/C system operates according to the vapor-compression refrigeration cycle and comprises four thermodynamic processes undergone by the refrigerant, namely compression, condensation, expansion, and evaporation [2]. Under real operating conditions, the compressor is driven by a belt and pulley transmission system connected to the engine crankshaft, causing the compressor speed to vary continuously from approximately 950 rpm during engine idle conditions to 3000 rpm during on-road operation [3]. Consequently, compressor speed has a direct influence on the cooling capacity and energy consumption of the A/C system [4].

The compressor circulates the refrigerant through the A/C system and consumes energy to sustain the refrigeration cycle, thereby reducing the engine power available for vehicle propulsion. When the compressor is activated, the engine must increase its operating speed to meet the additional energy demand, which raises energy consumption by 3% to 20%, equivalent to approximately 0.2 to 1 L of fuel per 100 km in light-duty vehicles [5]. In compressors with a displacement of 210 cm^3, peak energy consumption can reach up to 6 kW [6].

The performance of automotive air conditioning systems is determined by the interaction among compressor type, refrigerant, lubricant, and system load conditions.

Santanu et al. [7] evaluated the effects of refrigerant charge, compressor speed, and evaporator airflow rate in an automotive A/C system using an experimental test bench operating with R-134a. The results showed that increasing the refrigerant charge raised the refrigerant mass flow rate and system pressure. Greater compressor speed increased the temperature and pressure in the compressor discharge region and improved the system cooling capacity. However, this also led to increased compressor power consumption, negatively affecting A/C system performance. Finally, they concluded that the optimal charge for the A/C system was 530 ±3 g of refrigerant, achieving greater cooling capacity at 1900 rpm and a higher COP at a compressor speed of 1600 rpm.

Macagnan et al. [8] studied the influence of refrigerant charge and compressor speed. The authors concluded that compressor speed can increase compressor work by up to 78% within the range of 1500 to 3500 rpm, while the COP tends to decrease as compressor revolutions increase. They also reported a slight increase in COP when the refrigerant charge in the system was increased.

Gomaa [9] conducted simulations to evaluate the performance of an automotive A/C system using several refrigerants proposed as alternatives to R-134a. The tests were performed at different compressor speeds, cabin temperatures, and condenser airflow rates. The results showed that a 5 °C increase in condenser air temperature decreased the cooling capacity by up to 27% when the system operated with R-134a. Increasing compressor speed raised the refrigerant mass flow rate in the evaporator and improved the cooling capacity. However, higher compressor speed is associated with greater friction and lower efficiency, which negatively affects the COP. The study also showed that R-1234ze has better thermal and environmental characteristics, while R-1234yf provides better thermal performance but requires system design modifications to compensate for reductions in COP and cooling capacity.

Lee et al. [10] conducted compressor design optimization studies using an experimental model and a simulation program to evaluate the effects of R-134a and R-1234yf within a compressor speed range of 1000 rpm to 4000 rpm, while controlling the evaporator temperature. The authors concluded that R-1234yf has a COP 5% lower than that of R-134a. By redesigning the compressor valves, the system improved its COP by up to 8% when the evaporator temperature was maintained at 5 °C. Increasing the compressor speed from 1000 to 2000 rpm enhanced the cooling capacity, whereas the COP decreased due to higher energy consumption. Within the speed range of 2000 to 4000 rpm, the COP decreased by 17%.

Alkan and Hosoz [11] compared fixed-displacement and variable-displacement compressors. They evaluated the compressors at different speeds and under different airflow rates through the evaporator and condenser. The results showed that the automotive A/C system with a fixed-displacement compressor, operating at 750 rpm, presented a cooling capacity that was 3.2% to 7.8% higher than that of the variable-capacity compressor. The system with a variable-capacity compressor had a lower COP at low rotational speeds, whereas at high speeds, it was more efficient than the system with a fixed-displacement compressor.

Shaker et al. [12] compared refrigerants intended to replace R-134a by implementing a test bench that simulated the operation of a single-stage heat pump at different compressor speeds. Pressure, temperature, and Coriolis-type flow sensors were installed, along with a frequency-controlled compressor operating at 35, 40, 45, and 50 Hz to simulate the behavior of R-1234yf and R-515B. The results showed that R-1234yf exhibited better cooling capacity performance. However, compressor work was also affected by the high

operating pressures. In addition, the operating temperatures of R-1234yf were 3 °C lower than those of R-515B, which may contribute to extending compressor life. Both refrigerants also had a lower global warming potential (GWP) than R-134a. For both refrigerants, increasing compressor speed enhanced cooling capacity because a greater amount of refrigerant circulated through the evaporator, which, in turn, implied higher compressor energy demand. Finally, R-515B offered lower cooling capacity but, due to its lower compressor work, maintained a COP that was 8% higher in cooling mode and 13% higher in heating mode than that of R-1234yf.

Alkan and İnan [13] conducted an experimental study showing that R-1234yf produced a 13.6% to 20.1% reduction in COP compared with R-134a in variable-capacity compressors, although it reduced exergy destruction in certain system components.

Zawawi et al. [14] demonstrated that lubricant selection is a determining factor in electric vehicle systems, since PAO-type oils provide greater efficiency, lower energy consumption, and higher cooling capacity than PVE and POE oils. Yusri et al. [15] analyzed the optimization of refrigerant volume and compressor oil in an automotive air conditioning system, demonstrating that these parameters directly influence system performance and dynamic behavior, and that efficiency can be improved through advanced statistical analysis and machine learning techniques. Overall, these results highlight the importance of integrating thermodynamic and operational variables into the design of automotive A/C systems to improve energy efficiency and performance.

The literature review reveals limited analysis of the influence of compressor speed on isentropic and volumetric efficiencies, which restricts the understanding of its effect on cooling capacity, energy consumption, and the performance of automotive A/C systems. Moreover, the experimental test benches used in previous studies do not control evaporator temperature, making it difficult to reproduce operating conditions similar to those of a real system. Finally, measurement limitations were identified due to physical factors, the limited number of measurement points, and the use of conventional sensors.

In the present work, an experimental test bench was developed to control compressor rotational speed and record temperature, pressure, and air velocity data through an automated real-time data acquisition system. The test bench includes a thermal chamber to control the inlet air temperature at the evaporator. In addition, the increase in fuel consumption associated with air conditioning operation is calculated, and correlations are proposed to estimate the compressor isentropic and volumetric efficiencies as functions of operating parameters such as rotational speed and pressure ratio.

2. Materials and Methods

2.1. Experimental Test Bench of the Automotive A/C System

The experimental test bench is a system designed to simulate and evaluate the operation of the automotive A/C system under controlled conditions. Figure 1 illustrates the experimental test bench, which consists of the refrigeration circuit, the compressor drive system, and the control and instrumentation system.

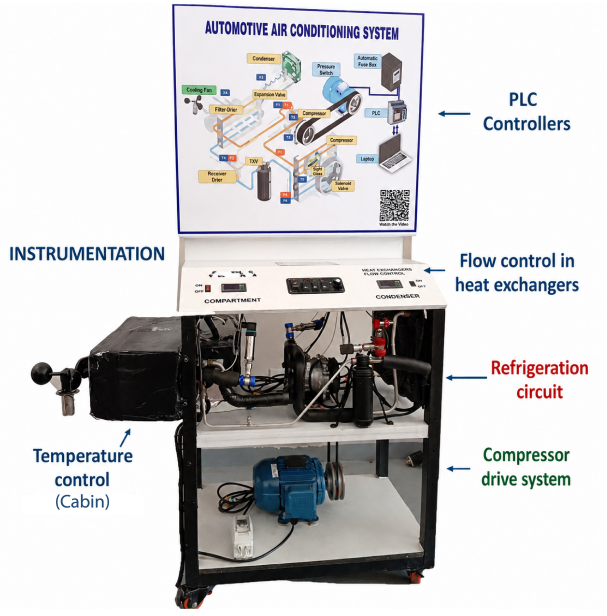

Figure 1. Experimental test bench of the automotive A/C system.

2.1.1. Refrigeration Circuit

The refrigeration circuit consists of an 87 cm^3 SD5H09 A/C compressor, a 3.5 m^2 evaporator with a cooling capacity of 12000 BTU (3.5 kW), a 7.2 m^2 condenser, a TI(E)1/20A5TR thermostatic expansion valve, a 515-3R external filter drier with switch, R-134a refrigerant, and PAG 100 compressor oil with a charge of 4.5 to 5 oz. The evaporator air blower is rated at 80 W and reaches 3800 rpm, controlled by a three-speed potentiometer, whereas the condenser fans are rated at 80 W and reach maximum speeds of 2250 rpm and 2100 rpm.

2.1.2. Compressor Drive System

Figure 2 shows the implementation of the compressor drive system. In internal combustion engine (ICE) vehicles, compressor speed depends on engine rotational speed, whereas in electric vehicles, it depends on the thermal demand of the cabin. In the experimental test bench, the compressor is driven by a 2.2 kW WEG-W22 three-phase electric motor through pulleys and

a V-belt with a tensioner. The electric motor speed is controlled by a KEWO-AD350 frequency inverter and SIEMENS LOGO 8 programmable logic controller (PLC) modules. Communication is performed through a 0 to 10 V analog reference signal sent by the PLC module, allowing the compressor speed to be controlled from a computer linked to the experimental test bench program.

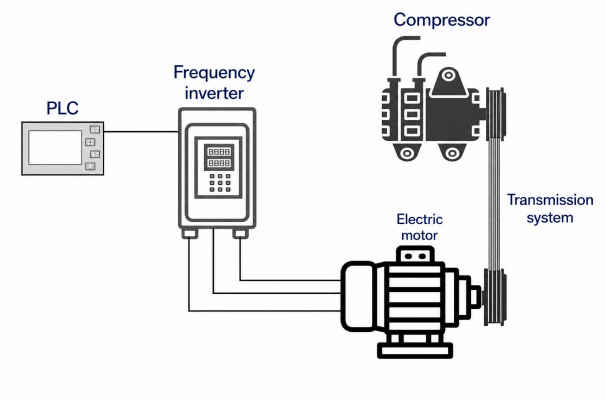

Figure 2. Compressor drive system.

The electric motor was sized by determining the compressor power consumption ($\dot{W}_m$) through an energy balance expressed in Equation (1), in which the isentropic compressor work, the isentropic efficiency (η_{iso}), and a heat loss coefficient to the environment (ϵ) due to natural convection in the compressor are considered [16].

$$\dot{W}_{comp} = \frac{\dot{m}(h_{2s} - h_1)}{\eta_{iso}(1 - \epsilon)} \tag{1}$$

The power supplied to the drive system ($\dot{W}_m$) is calculated considering the efficiencies of the electric motor (η_m) and the transmission system (η_p), as given in Equation (2) [16].

$$\dot{W}_m = \frac{\dot{W}_{comp}}{\eta_p * \eta_m} \tag{2}$$

Equation (3) expresses the dynamic analysis of the transmission system, where N_m is the rotational speed of the motor pulley, D_{pm} is the diameter of the motor pulley, N_c is the rotational speed of the compressor pulley, and D_{pc} is the diameter of the compressor pulley.

$$N_m * D_{pm} = N_c * D_{pc} \tag{3}$$

2.1.3. Instrumentation and Control System

The experimental test bench is designed to control compressor speed, cabin temperature, and airflow through the evaporator and condenser using the following systems.

Cabin Temperature Control

To simulate the temperature reached inside the cabin, a thermal chamber controlled by a PID controller was developed to activate and deactivate a direct-current electric resistance, generating up to 1000 W of power to heat the air entering the evaporator, as shown in Figure 1.

Airflow Control Through the Heat Exchangers

The airflow through the evaporator is controlled by a circuit that adjusts the electric fan speed across three levels, while the condenser airflow is controlled by a second fan activated by an STC 1000 PID controller when the condensation temperature configured in the test bench is reached.

Instrumentation and Data Acquisition

Four pressure sensors (P) were installed downstream of each component of the refrigeration circuit. Eight temperature sensors (T) were installed: four in the refrigeration circuit (1–4), one on the compressor casing (5), one at the evaporator air inlet (7), one at the evaporator air outlet (6), and one at the condenser air outlet (8). In addition, an anemometer was installed to measure the velocity of the air leaving the evaporator, as shown in Figure 3.

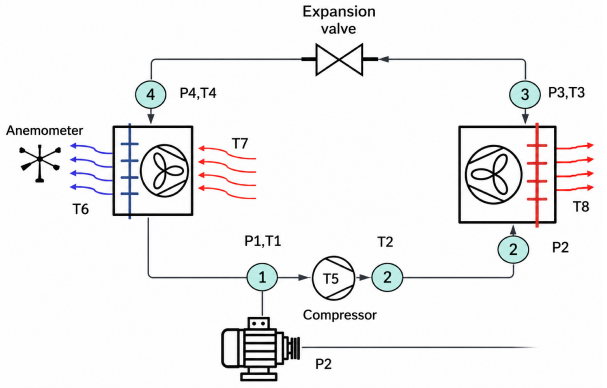

Figure 3. Sensors installed in the experimental test bench.

The PLC modules operate with analog and digital signals from 0 to 10 volts; therefore, the sensor signals must remain within the PLC operating range. The pressure sensors generate a 4 to 20 mA current signal, which is converted to a voltage range of 1.32 to 6.6 V through a 330 Ω resistance circuit.

The PT100 resistive temperature sensors change their resistance as a function of temperature and, when connected to an RTD transmitter, generate a 0 to 10 V signal. The anemometer is self-generating, does not require an external power supply, and produces a 0 to 2 V signal.

Monitoring, control, and data acquisition are performed using PLC modules (LOGO 8 12/24 RCE) and their corresponding expansion modules (AM2, AM2 AQ, AM2 RTD). The program was developed using LOGO Soft Comfort V8 software. In this program, the sensors were calibrated, analog signals were converted into measurement units, frequency inverter control was established, and data logging was configured. The monitoring interface was designed using LOGO Web Editor V1.1.0 (LWE) software [17]. This interface enables sensor monitoring, frequency inverter management, and data logging. Finally, the drive system equipment and sensors were calibrated and verified using equipment datasheets and reference instruments to ensure proper operation and result accuracy.

The uncertainty analysis of the measurements was performed according to the international ISO/IEC standard [18]. The combined (μ_c) and expanded (U_c) sensor uncertainties were evaluated, considering the uncertainty of each sensor (μ_s), the PLC uncertainty (μ_{PLC}) associated with the 10-bit ADC, and the repeatability uncertainty (μ_r) for 10 repetitions. Table 1 summarizes the sensor uncertainties.

Table 1. Sensor Uncertainties

Sensor	Tolerance	μ_s	μ_{PLC}	μ_r	μ_c	U_c
PT100 Temperature (-100°C–200°C)	± 0.3 °C	0.173 °C	0.085 °C	0.081 °C	0.209 °C	±0.418 °C
HK1100C pressure transducer (0–1.2 MPa)	± 1.5% FS ±0.018 MPa	0.0104 MPa	0.00034 MPa	0.00069 MPa	0.0104 MPa	±0.0208 MPa
DIY Anemometer (0–30 m/s)	±0.3 m/s	0.173 m/s	0.0085 m/s	0.068 m/s	0.186 m/s	±0.372 m/s

Sensor calibration was performed according to ISO/IEC Guide 99:2007 [19]. The PT100 sensors were calibrated in accordance with IEC 60751:2022 [20] by comparison with a reference standard thermometer (PIDMaxwell MLC-48) inside the thermal chamber, using two calibration points, 35 °C and 40 °C, which cover the operating range of the vehicle cabin. The maximum observed deviation was ±1 °C, within the specified class B tolerance. The HK1100C pressure sensors were calibrated according to IEC 62828-2:2017 [21], with a maximum observed deviation of ±0.021 MPa. Meanwhile, the DIY anemometer was calibrated by comparison with an Extech AN100-NIST anemometer, with a maximum observed deviation of ±0.25 m/s.

2.2. Experimental Campaign

The tests conducted on the experimental test bench represent real operating conditions of the A/C system in light-duty vehicles, as shown in Table 2.

Table 2. Test Matrix

Temperature in the passenger compartment (°C)	Compressor speed compressor (RPM)	Flow rate evaporator (m^3/h)	Flow rate condenser (m^3/h)
35–40–45	900–2800	313	496

Table 2 shows the parameters configured in the experimental test bench for testing and data collection. The cabin temperature varied from 35 to 45 °C, a range that can be reached in Riobamba [22, 23]. Under real operating conditions, the compressor rotational speed is 900 rpm under idling conditions, 1800 rpm during urban driving, and up to 3000 rpm on highways [3, 4]. In addition, the evaporator airflow was maintained at its maximum capacity, while the condenser airflow was generated by a single fan.

Cabin temperature control is performed using an STC-1000 PID temperature controller, as shown in Figure 4 (A). Control of the evaporator airflow and the compressor electromagnetic clutch is performed from the panel shown in Figure 4 (B), while condenser airflow control is achieved using an STC-1000 PID temperature controller, as shown in Figure 4 (C).

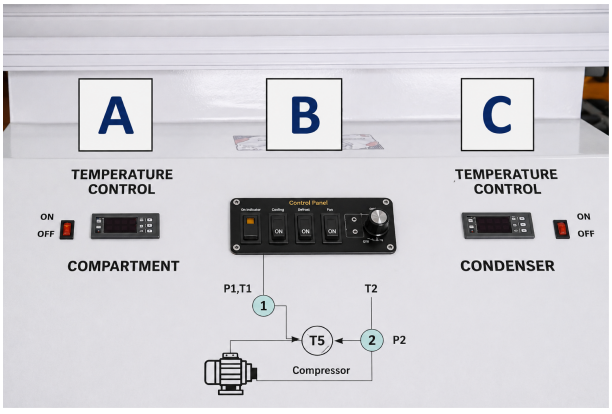

Figure 4. Experimental Test Bench Controls.

2.3. Thermodynamic Model of the Automotive A/C System

The data obtained from the experimental test bench sensors are recorded in a (.csv) file generated by LOGO

8 Soft Comfort software. To analyze the performance of the A/C system, the refrigerant mass flow rate delivered by the compressor, evaporator cooling capacity, compressor power consumption, and coefficient of performance (COP) must be calculated. To this end, a thermodynamic model was implemented considering energy transfers in the heat exchangers and compressor performance in terms of isentropic and volumetric efficiencies. The thermodynamic model is based on a steady-state analysis of an open system, assuming one-dimensional refrigerant flow and negligible variations in kinetic and potential energy. Heat losses to the surroundings are considered negligible, except in the heat exchangers and the compressor. Thermophysical properties are obtained from the NIST database [24]. The compressor is modeled using isentropic and volumetric efficiencies [16], while the heat exchangers are analyzed using energy balances based on the calorimetric method [25]. Isenthalpic expansion is assumed in the thermostatic expansion valve, and pressure losses in pipes and fittings are considered negligible compared with those of the main components.

The refrigerant mass flow rate was calculated through an energy balance in the evaporator, according to Equation (4) and based on the calorimetric method described in EN 13771-1 [25], where $\dot{m}_{ref}$ is the refrigerant mass flow rate, $\dot{m}_{air}$ is the air mass flow rate, ΔT_{6-7} is the temperature difference between the inlet and outlet air of the evaporator, as shown in Figure 3, Cp_{air} is the specific heat of air, and Δh_{1-4} is the refrigerant enthalpy difference between the inlet and outlet of the evaporator.

$$\dot{m}_{ref} = \frac{\dot{m}_{air} * Cp_{air} * \Delta T_{6-7}}{\Delta h_{1-4}} \tag{4}$$

The air mass flow rate is calculated from the volumetric airflow rate and air density, as given in Equation (5). The volumetric airflow rate is determined by multiplying the airflow passage area at the evaporator outlet (A_{air}), the density of the air leaving the evaporator (ρ_{air}), and the flow velocity ($\vec{V}_{air}$) measured by the anemometer, as shown in Figure 3 [2].

$$\dot{m}_{air} = \rho_{air} * A_{air} * \vec{V}_{air} \tag{5}$$

The evaporator cooling capacity ($\dot{Q}_{evap}$) is calculated using Equation (6) [16].

$$\dot{Q}_{evap} = \dot{m}_{ref} * (h_1 - h_4) \tag{6}$$

The volumetric efficiency (n_v) represents the relationship between the theoretical and actual capacity of the compressor to drive the refrigerant through the system. It is calculated using Equation (7) [16], [23], where $\dot{V}_s$ is the volumetric displacement of the compressor and ρ_{in} is the density of the refrigerant entering the compressor.

$$n_v = \frac{\dot{m}_{ref}}{\rho_{in} * \dot{V}_s} \tag{7}$$

The compressor isentropic efficiency (η_{iso}) represents the relationship between the ideal and actual energy required to compress the refrigerant. It is calculated using Equation (8) [16] [23], where h_1 is the refrigerant enthalpy at the compressor suction, h_{2s} is the discharge enthalpy during isentropic compression, and h_2 is the discharge enthalpy during actual compression.

$$\eta_{iso} = \frac{h_{2s} - h_1}{h_2 - h_1} \tag{8}$$

The energy consumed by the compressor is greater than the energy transferred to the refrigerant because of heat losses ($\dot{Q}_p$) caused by system irreversibilities. The heat rejected from the compressor to the surroundings is calculated using Equation (9) [26], where h_{amb} is the natural convection coefficient, A_c is the compressor surface area, T_s is the compressor casing temperature, and T_{amb} is the ambient temperature.

$$\dot{Q}_p = h_{amb} * A_c * (T_s - T_{amb}) \tag{9}$$

The work transferred to the refrigerant ($\dot{W}_{fluid}$) is determined using Equation (10).

$$\dot{W}_{fluid} = \dot{m}_{ref} * (h_2 - h_1) \tag{10}$$

The compressor heat rejection coefficient (ϵ_{Qp}) is calculated using Equation (11) [27].

$$\epsilon_{Qp} = \frac{\dot{Q}_p}{\dot{W}_{fluid} + \dot{Q}_p} \tag{11}$$

The compressor energy consumption is calculated using Equation (12).

$$\dot{W}_c = \frac{\dot{m}_{ref}(h_{2s} - h_1)}{\eta_{iso}(1 - \epsilon_{Qp})} \tag{12}$$

Finally, the system COP is used to evaluate the operating efficiency of the automotive A/C systemby relating the cooling capacity to the compressor energy consumption. It is calculated using Equation (13).

$$COP = \frac{\dot{Q}_{evap}}{\dot{W}_c} \tag{13}$$

Fuel consumption associated with air conditioning operation is estimated by considering the energy transformations in a gasoline-powered internal combustion engine (ICE) vehicle, as shown in Figure 5. This transformation begins in the internal combustion engine, which converts fuel energy into thermal energy and subsequently into mechanical energy at the crankshaft. These energy transformations have efficiencies between 27% and 30% [28]. Losses also occur in the transmission mechanisms connecting the crankshaft

to the compressor, with efficiencies between 80% and 93% [29].

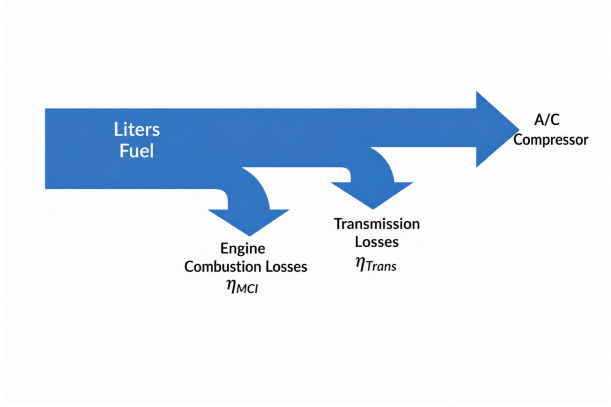

Figure 5. Energy transformation in an ICE vehicle for compressor operation [30].

The energy delivered by the fuel (E_{tot}) is calculated by dividing the energy consumed by the compressor (E) by the internal combustion engine efficiency (η_{MCI}) and the transmission efficiency (η_{trans}), as given in Equation (14).

$$E_{tot} = \frac{E}{\eta_{MCI} * \eta_{trans}} \tag{14}$$

Fuel consumption in liters (l_{fuel}) is obtained by dividing (E_{tot}) by the fuel lower heating value (PCI_{fuel}) and the fuel density (ρ_{fuel}), as given in Equation (15).

$$l_{fuel} = \frac{E_{tot}}{PCI_{fuel} * \rho_{fuel}} \tag{15}$$

An LHV of 46522.5 kJ/kg and a density of 739 kg/m^3 were used for gasoline [31].

3. Results and Discussion

A total of 60 experimental points were obtained according to the test matrix in Table 2 to analyze the influence of compressor speed and cabin temperature on compressor operation and automotive A/C system performance. To validate the results, the experimental values were compared with those predicted by the thermodynamic model. The percentage deviations were 1.66% for the COP, 4.85% for cooling capacity, 4.91% for compressor power, 4.86% for refrigerant mass flow rate, 3.08% for isentropic efficiency, and 9.83% for volumetric efficiency. Likewise, the overall energy balance showed a closure error of 6.05%. The observed differences are mainly attributed to measurement uncertainties, model simplifications and unaccounted thermal losses. Overall, these results demonstrate good agreement between the model and the physical behavior of the system.

3.1. Compressor Performance

3.1.1. Compressor Discharge Temperature

Figure 6 shows that the compressor discharge temperature rises as the compressor rotational speed increases. At a cabin temperature of 35 °C, the discharge temperature increases by 34.3%, from 58.16 °C to 78.13 °C, within the range of 900 to 2800 rpm. Similar results were also reported in [12].

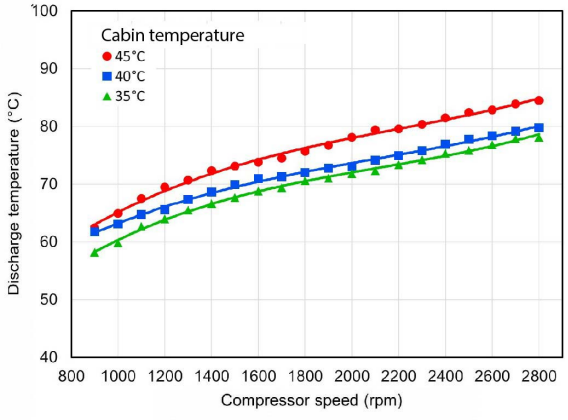

Figure 6. Discharge temperature as a function of compressor speed.

The compressor discharge temperature increases by 4.3 to 7.1 °C when the cabin temperature rises by 10 °C. However, the temperatures reached remain within the safe operating range, below 115 °C, preventing possible lubricating oil degradation that could compromise the mechanical integrity of the compressor.

This behavior occurs because increasing compressor speed raises the compression work and, consequently, the energy transferred to the refrigerant, thereby increasing the discharge temperature. In addition, greater process irreversibilities and limited heat dissipation to the surroundings contribute to the observed temperature rise.

3.1.2. Refrigerant Mass Flow Rate

Figure 7 shows that, at a cabin temperature of 35 °C, the mass flow rate increases by 50.3% as the compressor speed rises from 900 to 2800 rpm, because the compressor drives a greater amount of refrigerant per unit time.

When the cabin temperature increases from 35 to 40 °C, the refrigerant mass flow rate rises by 16.8% at 900 rpm, 21.0% at 1800 rpm, and 22.5% at 2800 rpm. This trend indicates that refrigerant circulation increases as cabin temperature rises. When the air passing through the evaporator is hotter, the refrigerant has a higher density at the compressor inlet because its temperature and pressure increase, which,

according to Equation (7), raises the mass flow rate. Similar results were reported in [32].

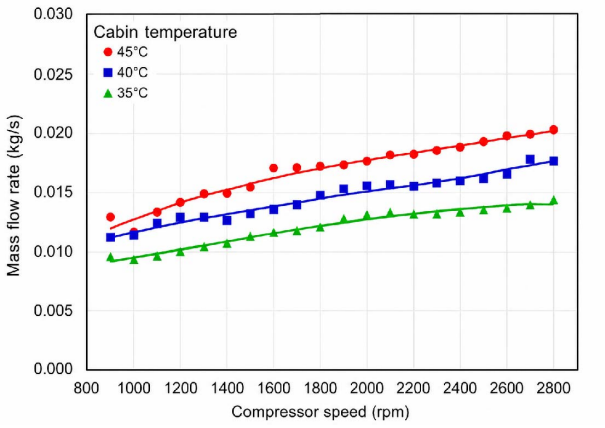

Figure 7. Refrigerant mass flow rate as a function of compressor speed.

From a physical perspective, the increase in refrigerant mass flow rate is directly related to the greater displaced volume per unit time and to variations in the thermodynamic properties of the refrigerant at the compressor suction, which increase refrigerant density and promote higher refrigerant circulation within the system.

3.1.3. Compressor Power Consumption

Figure 8 shows that as the compressor speed increases, a greater amount of energy is consumed. At a cabin temperature of 35 °C, the compressor power consumption increases from 0.287 kW to 0.878 kW when the speed rises from 900 to 2800 rpm. This increase is due to the greater amount of refrigerant driven by the compressor, as shown in Figure 7.

At high compressor speeds, the pressure ratio (PR) is greater, meaning that the compressor must reach a higher pressure in the high-pressure line, which increases the power required to compress the refrigerant. This behavior results from the higher pressure ratio, which raises the specific compression work, while the greater mass flow rate increases the total power requirement. Overall, these effects reflect increased irreversibilities and mechanical losses at high operating speeds.

When the cabin temperature increases from 35 to 40 °C, compressor power consumption also rises by 11.0%, 19.4%, and 20.6% at 900, 1800, and 2800 rpm, respectively. This increase becomes even more evident when the cabin temperature reaches 45 °C, because the cooling demand increases and a greater refrigerant mass flow rate must be compressed, as shown in Figure 7.

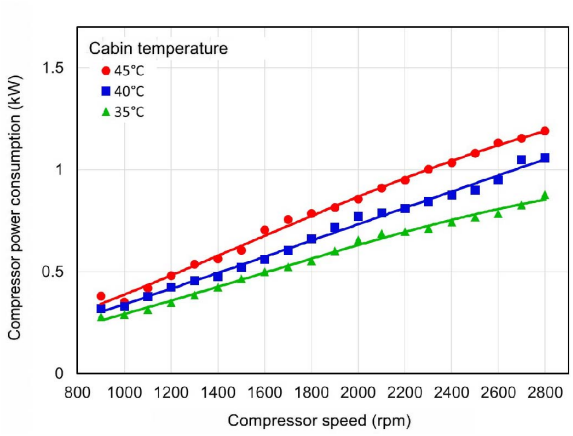

Figure 8. Compressor power consumption as a function of compressor speed.

3.1.4. Compressor Isentropic Efficiency

Figure 9 shows that isentropic efficiency decreases as compressor speed increases. At a cabin temperature of 35 °C, isentropic efficiency decreases by 22.66% when compressor speed rises from 1000 to 2800 rpm. Energy losses occur due to isenthalpic pressure drops in the suction valve, which generate flow turbulence, reduce compressor capacity, and increase energy consumption. This effect also occurs in the discharge valve [9]. Another contributing factor is the energy released by the compressor as heat. From a thermodynamic perspective, the decrease in isentropic efficiency is associated with increased internal irreversibilities, such as friction, turbulence, and thermal losses, which intensify as compressor operating speed increases.

When the cabin temperature increases from 40 to 45 °C, the efficiencies tend to decrease slightly, by 2.7% at 1000 rpm and 1% at 2800 rpm. As the temperature of the air passing through the evaporator increases, the refrigerant evaporation temperature and pressure also rise, increasing losses associated with pressure drops and heat transfer.

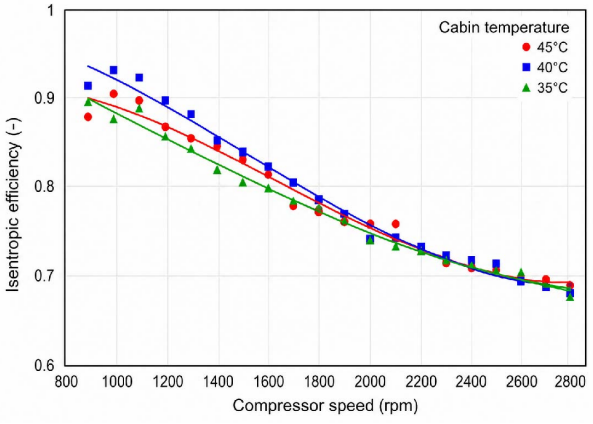

Figure 9. Isentropic efficiency as a function of compressor speed.

To provide a simple mathematical function for estimating compressor efficiency under different operating conditions, a linear regression was performed by correlating isentropic efficiency with compressor speed (ω_{comp}) and pressure ratio (PR), as given in Equation (16).

$$\eta_{iso} = 1.1905 + 0.000071\omega_{comp} - 0.1295PR \quad (16)$$

Figure 10 illustrates the comparison between the experimental isentropic efficiency values and those calculated using correlation (16). The results show a good fit for all points, with a maximum deviation of ±7% and a correlation coefficient r^2 of 0.914. The proposed correlation can be used to model compressor behavior in automotive A/C systems and predict compressor energy consumption.

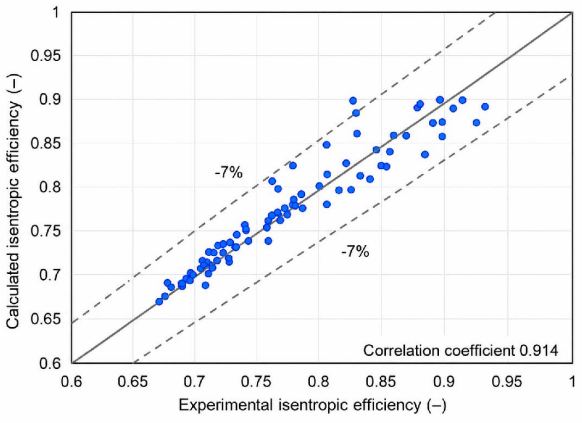

Figure 10. Comparison of the experimental and calculated values of compressor isentropic efficiency.

3.1.5. Compressor Volumetric Efficiency

Figure 11 shows that volumetric efficiency decreases as compressor rotational speed increases. At a cabin temperature of 35 °C, volumetric efficiency decreases by 44% within the range of 900 to 2800 rpm. Similar results were also reported in [33]. This behavior can be attributed to increased internal leakage, recirculation losses, and refrigerant compressibility effects, which become more significant at high speeds, reducing the effective suction capacity of the compressor.

An increase of 5 °C in cabin temperature results in a volumetric efficiency increase of 9.5% and 12.6% at 900 and 2800 rpm, respectively. This behavior occurs because the compressor heats up due to the refrigerant compression process and friction between the mechanical components. At higher compressor speeds, heat generation also increases. This heat is transferred to the compressor casing and to the suction and discharge ducts; consequently, the refrigerant expands reducing its density and decreasing the amount of refrigerant displaced by the compressor. In addition, compressors operate with a pressure difference between the suction and discharge sides, generating leakage of approximately 4.80% in the valve seating area [33]. This effect becomes more critical as the compressor rotational speed increases, since the pressure ratio (PR) also rises. Similarly, the pressure ratio produces greater pressure losses between the cylinder wall and the piston, negatively affecting volumetric efficiency [32]. Another factor influencing efficiency occurs during compression, when a small portion of the refrigerant tends to condense and then re-evaporate during suction, leading to the formation of liquid particles that increase the dead volume inside the cylinder. This effect is referred to as recirculating mass [33].

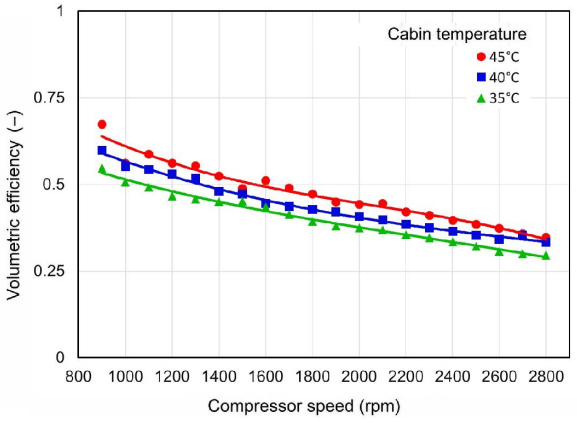

Figure 11. Volumetric efficiency as a function of compressor speed.

To determine a correlation for compressor volumetric efficiency, a regression was performed as a function of compressor speed (ω_{comp}), pressure ratio (PR), evaporation temperature ($T_{sat;evap}$), and refrigerant superheating at the evaporator outlet (SH), as given in Equation (17). The variables $T_{sat;evap}$ and SH are included in the correlation because refrigerant density changes at the compressor suction, directly affecting the displaced mass flow rate and, consequently, volumetric efficiency. When the system operates with high SH values, density varies at the same evaporation pressure. Therefore, considering only, the PR is insufficient, and SH and $T_{(sat;evap)}$ must also be included in the equation.

$$\begin{aligned}\eta_v = {} & 0.2576 + 0.000056\,\omega_{\text{comp}} - 0.0797\,PR \\ & + 0.01881\,T_{\text{sat,evap}} \\ & + 0.01908\,SH\end{aligned} \quad (17)$$

Figure 12 illustrates the comparison between the experimental volumetric efficiency values and those calculated using correlation (17).

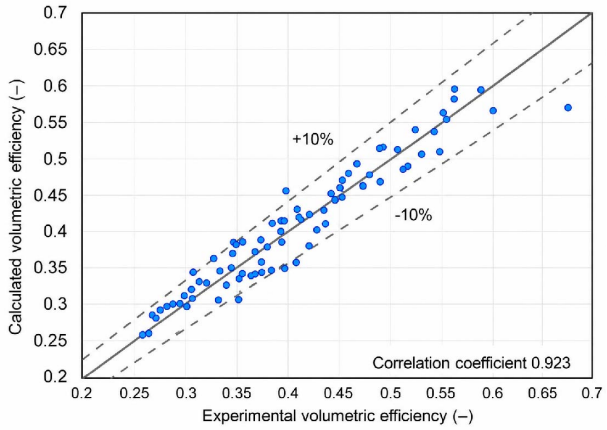

Figure 12. Comparison of the experimental and calculated values of compressor volumetric efficiency.

The results show a good fit for all points, with a maximum deviation of ±10% and a correlation coefficient r^2 of 0.923. The proposed correlation can be used to model compressor behavior in automotive A/C systems and predict the mass flow rate displaced by the compressor.

3.2. Performance of the Automotive A/C System

3.2.1. Cooling Capacity

Figure 13 shows that cooling capacity rises with increasing compressor rotational speed.

At a cabin temperature of 40 °C, increasing compressor speed from 900 to 2800 rpm raises the cooling capacity by 24.3%, whereas at 35 °C, the increase is 22.4%. Higher compressor speed leads to greater refrigerant circulation through the evaporator.

Cabin temperature also influences cooling capacity; greater cooling capacities are obtained as cabin temperature increases due to the higher mass flow rate as shown in Figure 7. Similar results were reported in [32] and [34].

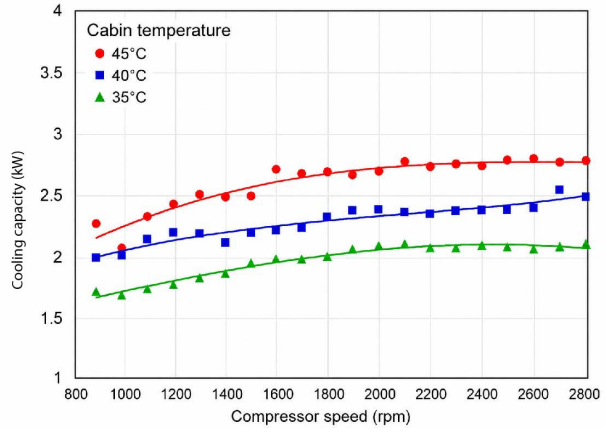

Figure 13. Cooling capacity as a function of compressor speed.

3.2.2. Coefficient of Performance (COP)

Figure 14 shows that, at a cabin temperature of 35 °C, the COP decreases by up to 61.27% as compressor rotational speed increases from 900 to 2800 rpm. Although the cooling capacity improves at higher compressor rotational speeds, power consumption also increases significantly, thereby reducing the system COP.

At higher speeds, greater energy losses occur due to friction in the moving components of the compressor, which reduces the COP [9]. When the cabin temperature increases from 40 °C to 45 °C, the COP decreases by 4.86% at 900 rpm and by 1.02% at 2800 rpm. However, cabin temperature has a smaller effect on the COP than on cooling capacity and compressor power consumption.

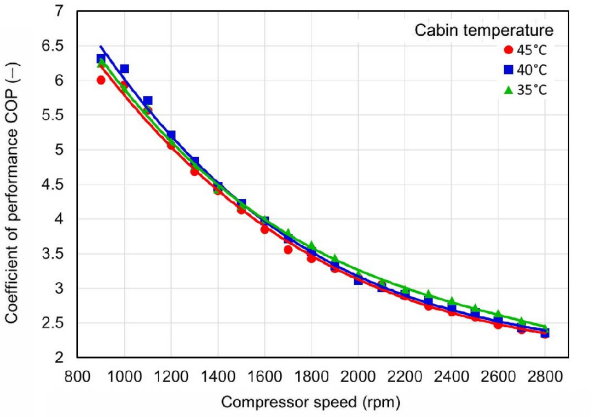

Figure 14. COP as a function of compressor speed.

3.2.3. Fuel Consumption

Figure 15 shows that fuel consumption rises when the engine operates at higher speed. At a cabin temperature of 45 °C, consumption increases by 213% from 900 to 2800 rpm because the compressor drives a greater amount of refrigerant.

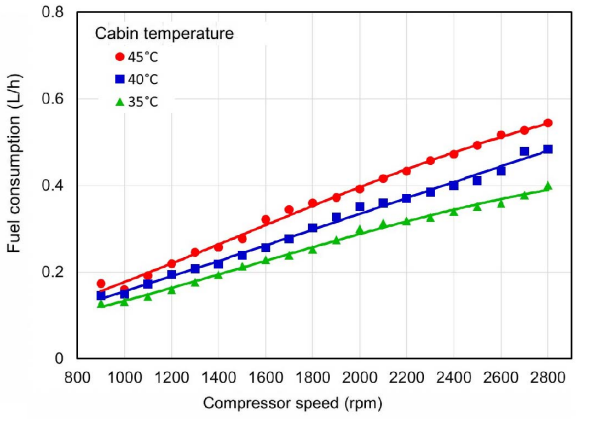

Figure 15. Fuel consumption of the automotive A/C system as a function of compressor speed.

As the cabin temperature increases, fuel consumption also rises. At 2800 rpm, corresponding to highway conditions, consumption increases from 0.40 L/h at 35 °C to 0.54 L/h at 45 °C. Similar results were reported in [35].

4. Conclusions

Increasing compressor speed raises the refrigerant mass flow rate, improving heat transfer capacity inside the vehicle. However, it also increases energy demand, leading to higher power and fuel consumption.

At a cabin temperature of 35 °C, increasing compressor speed from 900 to 2800 rpm raises the refrigerant mass flow rate by 50.3% and power consumption from 0.287 to 0.878 kW. Under the same conditions, compressor isentropic efficiency decreases by 22.66%, while volumetric efficiency decreases by 44%.

The compressor discharge temperature increases at higher rotational speeds, exceeding 80 °C. At a cabin temperature of 35 °C, increasing compressor speed from 900 to 2800 rpm raises the cooling capacity by 22.4%, whereas the system COP decreases by up to 61.27%. Although cooling capacity improves at higher compressor rotational speeds, power consumption also increases significantly, thereby reducing the system COP.

Fuel consumption doubles when compressor speed increases from 900 to 2800 rpm at a cabin temperature of 45 °C, reaching an instantaneous consumption of 0.54 L/h at 2800 rpm.

Contributor role

- **Iván M. Ashqui-Cuvi:** Data curation, formal analysis, validation, writing – original draft.
- **Klever S. Morales-Morales:** Data curation, formal analysis, validation, writing – original draft.
- **Daniela C. Vásconez-Núñez:** Conceptualization, research, methodology, supervision, writing – review and editing of results analysis.
- **Fernando M. Tello-Oquendo:** Conceptualization, research, methodology, supervision, writing – review and editing of results analysis.
- **Fabián C. Gunsha-Maji:** Data curation, formal analysis, and methodology.

References

[1] ANSI/ASHRAE, *ANSI/ASHRAE Standard 55-2017: Thermal Environmental Conditions for Human Occupancy*, ASHRAE Std., 2017, accessed: 2026-05-19. [Online]. Available: https://upsalesiana.ec/ing36ar7r1

[2] Y. A. Cengel, M. A. Boles, and M. Kanoglu, *Termodinámica*, 9th ed. Madrid: McGraw-Hill Education, 2019. [Online]. Available: https://upsalesiana.ec/ing36ar7r2

[3] R. Mcenaney, D. E. C. Boewe, J. M. Yin, Y. C. Park, C. Bullard, and P. S. Hrnjak, "Experimental comparison of mobile A/C systems when operated with transcritical CO_2 versus conventional R134A," in *Semantic Scholar*, 1998. [Online]. Available: https://upsalesiana.ec/ing36ar7r3

[4] Z. Diao, Y. Zhang, C. Li, X. Liu, and Z. Liu, "Dynamic characteristics of an automotive air-conditioning electromagnetic clutch," *Processes*, vol. 12, no. 1, p. 80, Dec. 2023. [Online]. Available: https://doi.org/10.3390/pr12010080

[5] S. Vashisht and D. Rakshit, "Recent advances and sustainable solutions in automobile air conditioning systems," *Journal of Cleaner Production*, vol. 329, p. 129754, Dec. 2021. [Online]. Available: https://doi.org/10.1016/j.jclepro.2021.129754

[6] NREL, "Significant fuel savings and emission reductions by improving vehicle air conditioning," National Renewable Energy Laboratory, Tech. Rep., 2004, presented at the 15th Annual Earth Technologies Forum and Mobile Air Conditioning Summit. [Online]. Available: https://upsalesiana.ec/ing36ar7r6

[7] S. P. Datta, P. K. Das, and S. Mukhopadhyay, "Effect of refrigerant charge, compressor speed and air flow through the evaporator on the performance of an automotive air conditioning system," *Proceedings of the International Refrigeration and Air Conditioning Conference (IRACC)*, 2014, paper No. 2399. [Online]. Available: https://upsalesiana.ec/ing36ar7r7

[8] M. Macagnan, J. Copetti, R. Souza, R. Reichert, and M. Amaro, "Analysis of the influence of refrigerant charge and compressor duty cycle in an automotive air conditioning system," in *Conference: 22nd International Congress of Mechanical Engineering (COBEM 2013)*, 12 2013. [Online]. Available: https://upsalesiana.ec/ing36ar7r8

[9] A. Gomaa, "Performance characteristics of automotive air conditioning system with refrigerant R134a and its alternatives," *International Journal of Energy and Power Engineering*, vol. 4, no. 3, p. 168, 2015. [Online]. Available: https://doi.org/10.11648/j.ijepe.20150403.15

[10] T. Lee, K.-H. Shin, J. Kim, D. Jung, and J.-H. Kim, "Design optimization of external variable displacement compressor with R1234yf for vehicle air conditioning system," *Applied Thermal Engineering*, vol. 198, p. 117493, Nov. 2021. [Online]. Available: https://doi.org/10.1016/j.applthermaleng.2021.117493

[11] R.-F. Horng, Y.-P. Chang, and S.-C. Wu, "Investigation on the production of hydrogen rich gas in a plasma converter for motorcycle applications," *Energy Conversion and Management*, vol. 47, no. 15-16, pp. 2155–2166, 2006. [Online]. Available: https://doi.org/10.1016/j.enconman.2005.12.010

[12] A. K. S. Al-Sayyab, J. Navarro-Esbrí, A. Barragán-Cervera, and A. Mota-Babiloni, "Effect of compressor speed on heat pump performance with climate-friendly refrigerants," *International Journal of Refrigeration*, vol. 177, pp. 296–304, 2025. [Online]. Available: https://doi.org/10.1016/j.ijrefrig.2025.05.027

[13] A. Alkan and M. S. İnan, "Experimental investigation of the effects of compressor types on the performance of an automobile air conditioning system using R1234yf," *International Journal of Refrigeration*, vol. 155, pp. 58–66, Nov. 2023. [Online]. Available: https://doi.org/10.1016/j.ijrefrig.2023.09.004

[14] N. N. M. Zawawi, A. R. M. Aminullah, W. H. Azmi, and H. M. Ali, "Performance comparison of electric vehicle air-conditioning system using R1234yf with various compressor lubricants," *Applied Thermal Engineering*, vol. 288, p. 129652, Mar. 2026. [Online]. Available: https://doi.org/10.1016/j.applthermaleng.2025.129652

[15] K. Zhang, D. Wu, K. Xu, and F. Zhan, "Design method for improving the electromagnetic and temperature performance of the four-way valve," *International Journal of Refrigeration*, vol. 154, pp. 19–32, Oct. 2023. [Online]. Available: https://doi.org/10.1016/j.ijrefrig.2023.07.018

[16] American Society of Heating, Refrigerating and Air-Conditioning Engineers, *ASHRAE Handbook—HVAC Systems and Equipment (SI Edition)*. Atlanta, GA, USA: ASHRAE, 2024. [Online]. Available: https://upsalesiana.ec/ing36ar7r16

[17] SIEMENS, *Ayuda en pantalla de LOGO Soft Comfort*, Siemens AG, 2022, software documentation / online help. [Online]. Available: https://upsalesiana.ec/ing36ar7r17

[18] ISO/IEC, *ISO/IEC Guide 98-1:2024 — Guide to the Expression of Uncertainty in Measurement — Part 1: Introduction*, ISO Std., 2024. [Online]. Available: https://upsalesiana.ec/ing36ar7r18

[19] ISO, *ISO/IEC Guide 99:2007: International Vocabulary of Metrology — Basic and General Concepts and Associated Terms (VIM)*, ISO Std., 2007, accessed: 2026-05-19. [Online]. Available: https://upsalesiana.ec/ing36ar7r19

[20] International Electrotechnical Commission (IEC), *IEC 60751:2022: Industrial Platinum Resistance Thermometers and Platinum Temperature Sensors*, IEC Std., 2022, accessed: 2026-05-19. [Online]. Available: https://upsalesiana.ec/ing36ar7r20

[21] ——, *IEC 62828-2:2017: Reference Conditions and Procedures for Testing Industrial and Process Measurement Transmitters – Part 2: Specific Procedures for Pressure Transmitters*, IEC Std., 2017, accessed: 2026-05-19. [Online]. Available: https://upsalesiana.ec/ing36ar7r21

[22] J. A. Chica Yuqui and M. P. Vinueza Cisneros, "Estudio de la influencia de la radiación solar en el calentamiento de vehículos tipo SUV," Riobamba, Ecuador, 2023. [Online]. Available: https://upsalesiana.ec/ing36ar7r23

[23] J. Trujillo Tello, C. Machado Solís, D. Vásconez Núñez, and F. Tello Oquendo, "Analysis of the thermal behavior of a vehicle cabin using a dynamic thermal model," *The Ecuadorian Journal of S.T.E.A.M.*, vol. 2, no. 4, pp. 1204–1217, 2021, accessed: 2026-05-19. [Online]. Available: https://doi.org/10.18502/espoch.v2i4.11747

[24] E. W. Lemmon, M. L. Huber, and M. O. McLinden, *NIST Standard Reference Database 23: Reference Fluid Thermodynamic and Transport Properties — REFPROP, Version 9.0*, National Institute of Standards and Technology, Gaithersburg, MD Std., 2010, accessed: 2026-05-19. [Online]. Available: https://upsalesiana.ec/ing36ar7r24

[25] European Committee for Standardization (CEN), *EN 13771-1:2017: Compressors and Condensing Units for Refrigeration — Performance Testing and Test Methods — Part 1: Refrigerant Compressors*, CEN Std., 2017, accessed: 2026-05-19. [Online]. Available: https://upsalesiana.ec/ing36ar7r25

[26] G. F. Nellis and S. A. Klein, *Heat Transfer*. New York, NY, USA: Cambridge University Press, 2009, accessed: 2026-05-19. [Online]. Available: https://upsalesiana.ec/ing36ar7r26

[27] E. Granryd, I. Ekroth, P. Lundqvist, Å. Melinder, B. Palm, and P. Rohlin, *Refrigerating Engineering*. Stockholm, Sweden: Royal Institute

of Technology (KTH), 2003. [Online]. Available: https://upsalesiana.ec/ing36ar7r27

[28] E. A. Llanes Cedeño, J. B. Carguachi-Caizatoa, and J. C. Rocha-Hoyos, "Evaluación energética y exergética en un motor de combustión interna ciclo Otto de 1.6l," *Enfoque UTE*, vol. 9, no. 4, pp. 221–232, Dec. 2018. [Online]. Available: http://doi.org/10.29019/enfoqueute.v9n4.365

[29] Megadyne, *Saving Energy with Efficient Belt Drives*. MegadyneGroup, 2025, e-book, Accessed: 2026-05-19. [Online]. Available: https://upsalesiana.ec/ing36ar7r29

[30] D. C. Vásconez Núñez, "Desarrollo de un modelo para el cálculo del consumo de climatización en vehículos de pasajeros urbanos." Ph.D. dissertation, Universitat Politecnica de Valencia, 2019. [Online]. Available: http://doi.org/10.4995/Thesis/10251/121133

[31] J. M. Mantilla González, B. J. Aguirre Junco, and S. P. L. Andrés, "Experimental evaluation of a spark-ignited engine using biogas as fuel," *Ingeniería e Investigación*, vol. 28, no. 2, pp. 131–141, 2008, accessed: 2026-05-19. [Online]. Available: https://upsalesiana.ec/ing36ar7r31

[32] J.M. Belman-Flores, J.M. Barroso-Maldondao, J.M. Mendoza-Miranda, A. Gallegos-Muñoz, J.M. Riesco Ávila, and C. Rubio-Maya, "Simulación energética de un aire acondicionado automotriz trabajando con refrigerantes R-1234yf y R-134a," *XIX Congreso Internacional Anual de la SOMIM*, 2013. [Online]. Available: https://doi.org/10.13140/2.1.2061.4725

[33] B. Tremeac, A. K. Datta, M. Hayert, and A. Le-Bail, "Thermal stresses during freezing of a two-layer food," *International Journal of Refrigeration*, vol. 30, no. 6, pp. 958–969, 2007. [Online]. Available: https://doi.org/10.1016/j.ijrefrig.2007.01.012

[34] J. Navarro-Esbrí, J. Mendoza-Miranda, A. Mota-Babiloni, A. Barragán-Cervera, and J. Belman-Flores, "Experimental analysis of R1234yf as a drop-in replacement for R134a in a vapor compression system," *International Journal of Refrigeration*, vol. 36, no. 3, pp. 870–880, May 2013. [Online]. Available: https://doi.org/10.1016/j.ijrefrig.2012.12.014

[35] C. Ding, T. Nie, and Y. Chen, "A distribution network solid-state DC circuit breaker with current limiting function," *Energy Reports*, vol. 8, pp. 986–994, Apr. 2022. [Online]. Available: https://doi.org/10.1016/j.egyr.2021.11.052